ELSEVIER

Thin-Walled Structures 40 (2002) 877–891

THIN-WALLED STRUCTURES

www.elsevier.com/locate/tws

Discontinuity effects at cone-cone axisymmetric shell junctions

A. Zingoni *

Department of Civil Engineering, University of Cape Town, Rondebosch 7701, Cape Town, South Africa

Received 5 August 2001; received in revised form 25 February 2002; accepted 5 March 2002

Abstract

In this paper, the problem of a conical shell axisymmetrically intersecting another conical shell, such that the vertices of the cones lie on opposite sides of the plane of intersection, is considered, and associated discontinuity effects quantified for arbitrary loading and geometric parameters of the intersecting cones. The ensuing very practical closed-form results are based on the one-term asymptotic-series solution for the axisymmetric bending of a non-shallow conical shell, and are intended for use in the quick evaluation of stresses and deformations in double-cone pressure vessels, as well as liquid-retaining vessels with intersecting conical portions. As an example of the application of the developed formulation, the stress distribution in a large liquid-filled elevated rhombic tank is evaluated. The stresses obtained on the basis of the closed-form analytical approach developed in the paper are shown to be in good agreement with those obtained from a finite-element analysis, confirming the reliability of the presented formulation.

Keywords: Axisymmetric bending of shells; Conical shell; Discontinuity stresses; Shell analysis; Shell junction; Shell of revolution

1. Introduction

Let us consider two conical shells axisymmetrically joined together along their open circular ends, as shown in Fig. 1.

* Tel.: +27-21-650-2601; fax: +27-21-689-7471.
E-mail address: azingon@eng.uct.ac.za (A. Zingoni).

0263-8231/02/$ - see front matter
PII: S0263-8231(02)00022-8

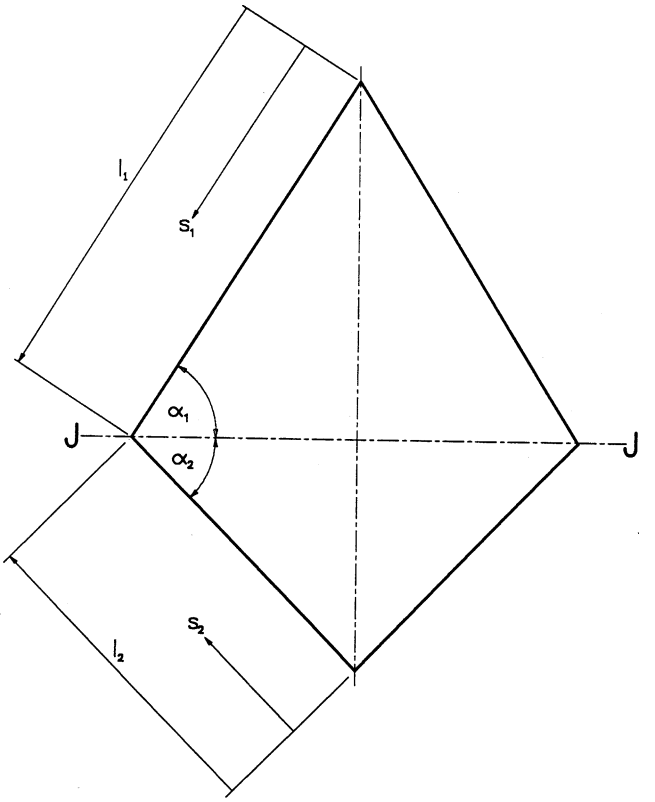

Fig. 1. Axisymmetrically intersecting conical shells with vertices lying on opposite sides of the plane of intersection.

For cone 1, the distance coordinate of a point on the shell meridian is s_1 ($0 \leq s_1 \leq l_1$) relative to the vertex of the cone, while for cone 2, the distance coordinate is s_2 ($0 \leq s_2 \leq l_2$). The angles of inclination of the straight meridians relative to the junction plane are α_1 and α_2 for cone 1 and cone 2, respectively. In general, $\alpha_1 \neq \alpha_2$ and $l_1 \neq l_2$.

The above configuration finds application in pressure-vessel technology as well as in constructions for liquid containment, typically elevated water-retaining tanks and innovative forms for sludge digesters. The last mentioned have been the subject of some recent studies [1–3].

The purpose of the present study is to quantify the discontinuity effects at the junction *JJ* of the two cones, for arbitrary loading and geometric parameters of the intersecting cones. Practical closed-form results are developed on the basis of the one-term asymptotic-series solution for the conical shell, and these results are simple, reliable and of fairly general applicability. As is usual for junction problems of the present type, the membrane solution for the shell is taken as the particular integral of the bending equations, and simply superimposed with the homogeneous solution

(corresponding to the application of axisymmetric bending moments and shearing forces at the shell edge in the absence of any surface loads). Discontinuity effects are evaluated through imposing conditions of geometric continuity and equilibrium at the shell junction, while net effects follow when membrane effects are superimposed with discontinuity effects. Such a flexibility-type approach is very fruitful in tackling statically indeterminate problems of shell bending, and has been amply illustrated in the literature [4–7].

2. Solution approach for the axisymmetric bending of the conical shell

Specialisation of the Reissner-Meissner pair of governing differential equations for the axisymmetric bending of shells of revolution, to the case of the conical shell of constant thickness t, yields the equations [6]

$$\frac{d^2V}{ds^2} + \frac{1}{s}\frac{dV}{ds} - \frac{1}{s^2}V = -\frac{Q_s}{D} \tag{1a}$$

$$\frac{d^2Q_s}{ds^2} + \frac{3}{s}\frac{dQ_s}{ds} = \frac{1}{s^2}(\tan^2\alpha)EtV \tag{1b}$$

where Q_s is the meridional transverse shearing force per unit length, V the rotation of the shell meridian, s the distance coordinate of a point on the shell meridian measured from the vertex of the cone, α the angle of inclination of the straight meridian relative to the plane perpendicular to the axis of revolution of the cone (refer to Fig. 1 for a depiction of s and α), D the flexural rigidity of the shell and E the Young modulus of the shell material. Like in the case of flat plates, the flexural rigidity of the shell is given by

$$D = \frac{Et^3}{12(1-\nu^2)} \tag{2}$$

where ν is the Poisson ratio of the material of the shell.

It is well known that the exact solution to Eqs. (1) may be obtained in terms of the Kelvin or Bessel functions [4,5]. However, the rigorous solution is not very well suited to practical engineering calculations, since it is too lengthy, even when tables of the Kelvin and/or Bessel functions are available. Flügge [5] has noted that sufficient accuracy is achieved by replacing the Bessel/Kelvin functions with their one-term asymptotic expansions, provided that $\omega \geq 15$, where ω is a geometrical parameter defined as follows:

$$\omega = 2\left[12(1-\nu^2)\left(\frac{s^2}{t^2}\right)\tan^2\alpha\right]^{1/4} \tag{3}$$

The condition $\omega \geq 15$ implies that

$$\frac{s}{t}\tan\alpha \geq \frac{16.24}{\sqrt{1-\nu^2}} \approx 17.0 \tag{4}$$

taking the more restrictive case of the material steel, between $\nu \approx 0.15$ for concrete and $\nu \approx 0.30$ for steel (if we confine our attention to these two commonest materials for shells of the type in question). Assuming that the cone is not 'too flat' (that is, assuming $\alpha \geq 30°$), it means that $(s/t) \geq 29.4 \approx 30$. The conditions $\alpha \geq 30°$ and $(s/t) \geq 30$ are satisfied by many conical shells encountered in practice, if we consider the ratio $s/t(\approx l/t)$ in the narrow zone of the shell edge experiencing 'edge effects' or 'bending disturbances'. This justifies the adoption of the one-term asymptotic-series solution, which leads to the results [6]

$$Q_s = \frac{1}{s\sqrt{2\pi\omega}}\, e^{\beta}\left[C_1\cos\left(\beta-\frac{\pi}{8}\right) + C_2\sin\left(\beta-\frac{\pi}{8}\right)\right] \tag{5a}$$

$$N_s = -Q_s\cot\alpha = -\frac{\cot\alpha}{s\sqrt{2\pi\omega}}\, e^{\beta}\left[C_1\cos\left(\beta-\frac{\pi}{8}\right) + C_2\sin\left(\beta-\frac{\pi}{8}\right)\right] \tag{5b}$$

$$N_\theta = -\left(\frac{\cot\alpha}{2s}\right)\left(\frac{\omega}{2\pi}\right)^{1/2} e^{\beta}\left[C_1\cos\left(\beta+\frac{\pi}{8}\right) + C_2\sin\left(\beta+\frac{\pi}{8}\right)\right] \tag{5c}$$

$$M_s = \frac{\sqrt{2}}{\omega\sqrt{\pi\omega}}\, e^{\beta}\left[C_1\sin\left(\beta+\frac{\pi}{8}\right) - C_2\cos\left(\beta+\frac{\pi}{8}\right)\right] \tag{5d}$$

$$M_\theta = \nu M_s \tag{5e}$$

$$V = \frac{1}{Et^2}\left[\frac{6(1-\nu^2)}{\pi\omega}\right]^{1/2} e^{\beta}\left[C_1\sin\left(\beta-\frac{\pi}{8}\right) - C_2\cos\left(\beta-\frac{\pi}{8}\right)\right] \tag{5f}$$

$$\delta = \frac{1}{Et}(s\cos\alpha)(N_\theta - \nu N_s) = -\frac{1}{Et}\frac{\cos\alpha\cot\alpha}{\sqrt{2\pi\omega}}\, e^{\beta} \times \left[\left\{\frac{\omega}{2}\cos\left(\beta+\frac{\pi}{8}\right)\right.\right. \tag{5g}$$

$$\left.\left. -\nu\cos\left(\beta-\frac{\pi}{8}\right)\right\}C_1 + \left\{\frac{\omega}{2}\sin\left(\beta+\frac{\pi}{8}\right) - \nu\sin\left(\beta-\frac{\pi}{8}\right)\right\}C_2\right]$$

where C_1 and C_2 are constants of integration. The parameter β is defined as

$$\beta = \frac{\omega}{\sqrt{2}} \tag{6}$$

while $\{N_s, N_\theta\}$ are stress resultants (forces per unit length) in the meridional and hoop directions respectively, $\{M_s, M_\theta\}$ are bending moments per unit length in the meridional and hoop sections respectively, and δ is the displacement of the shell in the direction perpendicular to the axis of revolution of the cone. The stress resultants $\{N_s, N_\theta\}$ are considered positive when tensile, while δ is considered positive when away from the axis of revolution of the shell. When the vertex of the cone is above the opening of the cone (as with cone 1 in Fig. 1), the meridional rotation V will be considered positive when anticlockwise as viewed to the left of the vertical axis of symmetry; when the vertex is below the opening of the cone (as with cone 2 in

Fig. 1), V will be considered positive when clockwise as viewed to the left of the axis. These and other sign conventions follow those adopted in Ref. [6].

As already stated, the homogeneous component of the total solution is associated with the application of axisymmetric actions along the shell edge, in the absence of any surface loads, while the particular solution is associated with the membrane state of stress as calculated for a given surface loading. The calculation of membrane effects for cones is relatively simple (see, for example, Ref. [6]), and these effects will therefore be assumed to be known for a given axisymmetric surface loading (such as uniform pressure, hydrostatic pressure or self-weight). This paper is primarily concerned with the quantification of the 'edge effects' or 'discontinuity effects' or 'bending disturbances' associated with the occurrence of edge redundants.

Let us assume that axisymmetric edge actions M_e (bending moment per unit length) and H_e (horizontal shearing force per unit length, if the axis of revolution of the cone is taken as vertical) occur as unknown redundants as shown in Fig. 2. For now, these are considered arbitrary; in due course, they will be evaluated on the basis of the physical conditions prevailing at cone-cone shell intersections.

For the case shown in Fig. 2a, the boundary conditions

$$(N_s)_{s=l} = 0 \tag{7a}$$

$$(M_s)_{s=l} = M_e \tag{7b}$$

lead to the results

$$C_1 = \frac{\omega_e\sqrt{\pi\omega_e}}{e^{\beta_e}}\left[\sin\left(\beta_e - \frac{\pi}{8}\right)\right]M_e \tag{8a}$$

$$C_2 = -\frac{\omega_e\sqrt{\pi\omega_e}}{e^{\beta_e}}\left[\cos\left(\beta_e - \frac{\pi}{8}\right)\right]M_e \tag{8b}$$

while for the case shown in Fig. 2b, the boundary conditions

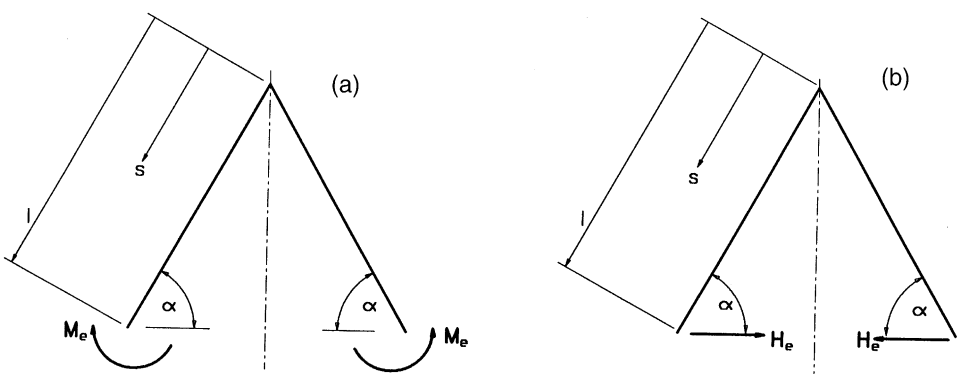

Fig. 2. Conical shell subjected to axisymmetric edge actions: (a) bending moment M_e; (b) horizontal force H_e (assuming that the axis of shell is vertical).

$$(N_s)_{s=l} = -H_e\cos\alpha \tag{9a}$$

$$(M_s)_{s=l} = 0 \tag{9b}$$

lead to the results

$$C_1 = \frac{2l(\sin\alpha)\sqrt{\pi\omega_e}}{e^{\beta_e}}\left[\cos\left(\beta_e + \frac{\pi}{8}\right)\right]H_e \tag{10a}$$

$$C_2 = \frac{2l(\sin\alpha)\sqrt{\pi\omega_e}}{e^{\beta_e}}\left[\sin\left(\beta_e + \frac{\pi}{8}\right)\right]H_e \tag{10b}$$

where the parameters ω_e and β_e denote the values of ω and β at the shell edge (that is, at $s = l$).

Note that the above expressions would not be applicable in the case of conical frusta, where the shell has two edges each associated with two boundary conditions, necessitating the retention of four constants of integration in the assumed one-term asymptotic-series solution. Baltrukonis [8] has given influence coefficients for edge-loaded 'short' conical frusta, on the basis of the one-term asymptotic expansions of the Kelvin functions. The term 'short' here implies that edge interaction cannot be ignored. However, in the case of frusta which are not too short (that is, where the length of the frustum is at least equal to the diameter of the smaller end of the frustum), the above expressions may be used at the larger end with good accuracy, as long as the earlier conditions that $\alpha \geq 30°$ and $(s/t) \geq 30$ are satisfied.

For the simultaneous application of M_e and H_e, use of results (8) and (10) in expressions (5) leads to the following closed-form expressions for interior stress resultants $\{N_s^b, N_\theta^b\}$ and interior bending moments $\{M_s, M_\theta\}$ in the shell, as well as for deformations V^b and δ^b evaluated at the shell edge (that is, V_e^b and δ_e^b):

$$N_s^b = -\left(\frac{\cot\alpha}{s\sqrt{2}}\right)\left(\frac{\omega_e}{\omega}\right)^{1/2} e^{-(\beta_e-\beta)}[\omega_e\{\sin(\beta_e-\beta)\}M_e + \sqrt{2}(l\sin\alpha)\{\cos(\beta_e-\beta)-\sin(\beta_e-\beta)\}H_e] \tag{11a}$$

$$N_\theta^b = -\left(\frac{\cot\alpha}{s2\sqrt{2}}\right)(\omega\omega_e)^{1/2} e^{-(\beta_e-\beta)}\left[\frac{\omega_e}{\sqrt{2}}\{\sin(\beta_e-\beta)-\cos(\beta_e-\beta)\}M_e + (2l\sin\alpha)\{\cos(\beta_e-\beta)\}H_e\right] \tag{11b}$$

$$M_s = \frac{\sqrt{2}}{\omega}\left(\frac{\omega_e}{\omega}\right)^{1/2} e^{-(\beta_e-\beta)}\left[\frac{\omega_e}{\sqrt{2}}\{\cos(\beta_e-\beta) + \sin(\beta_e-\beta)\}M_e - (2l\sin\alpha)\{\sin(\beta_e-\beta)\}H_e\right] \tag{11c}$$

$$M_\theta = \nu M_s \tag{11d}$$

$$V_e^b = \frac{1}{Et^2}[6(1-\nu^2)]^{1/2}[-\omega_e M_e + \sqrt{2}(l\sin\alpha)H_e] \tag{12a}$$

$$\delta_e^b = \left(\frac{\cos\alpha\cot\alpha}{4Et}\right)[\omega_e^2 M_e - 2\sqrt{2}(l\sin\alpha)(\omega_e - \nu\sqrt{2})H_e] \tag{12b}$$

The superscript b associated with $\{N_s^b, N_\theta^b\}$ and $\{V_e^b, \delta_e^b\}$ denotes effects associated with the bending-related edge actions M_e and H_e, as opposed to effects associated with the membrane solution, which will be denoted by the superscript m.

3. Application to pressurised rhombic shell of revolution

A rhombic shell of revolution (that is, two identical right cones connected at their open ends) under uniform internal pressure p is depicted in Fig. 3a. Each of the upper and lower halves of the vessel is an axisymmetric cone of length l and base angle α. Let us consider the equilibrium of an element of the shell at the junction of the two cones, when the edges of the cones are subjected to axisymmetric bending moments and shearing forces $\{M_e, H_e\}$ as depicted in Fig. 3b, while axisymmetric membrane meridional stress resultants N_{se}^m also occur at the shell edges as a result of the applied surface loading p (Fig. 3c). Horizontal equilibrium of the junction element requires that

$$2H_e - 2N_{se}^m\cos\alpha = 0 \tag{13}$$

leading to the result

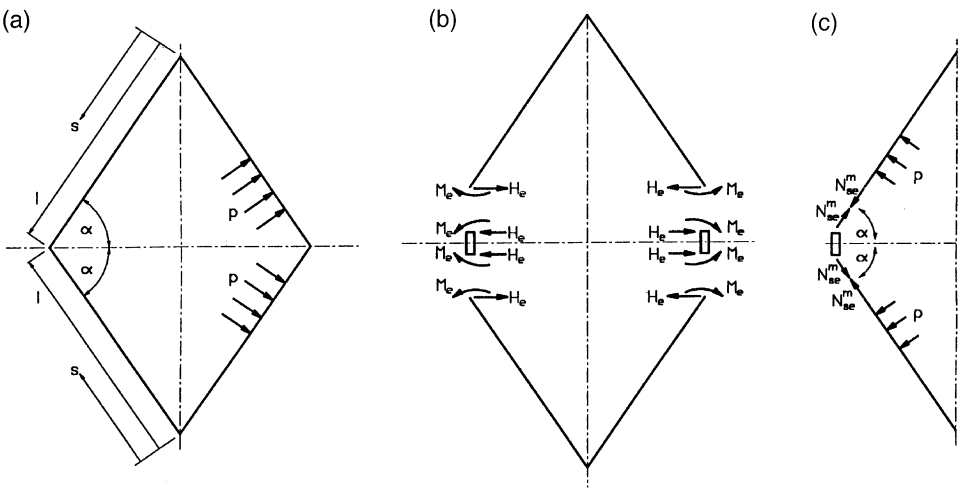

Fig. 3. Pressurised rhombic shell of revolution: (a) general arrangement; (b) shell-edge bending and shearing actions; (c) shell-edge membrane actions.

$$H_e = N_{se}^m \cos\alpha \tag{14}$$

Now, from considerations of the membrane theory of conical shells [6],

$$N_s^m = \frac{ps}{2}\cot\alpha \Rightarrow N_{se}^m = \frac{pl}{2}\cot\alpha \tag{15}$$

for the case of uniform internal pressure p, so that expression (14) becomes

$$H_e = \frac{pl}{2}\cot\alpha\cos\alpha \tag{16}$$

Also, rotation of the shell meridians may occur at the junction of the two cones, but the angle 2α between adjacent shell meridians (Fig. 3a) must remain unchanged, since the junction is monolithic (i.e. rigid). However, any such rigid-body rotation of the junction would violate the symmetry of the situation. It follows therefore that the net (i.e. total) rotation V_e^T of the shell edges under the simultaneous occurrence of the bending-related actions $\{M_e, H_e\}$ and the membrane effects must be zero. That is,

$$V_e^T \,(= V_e^b + V_e^m) = 0 \tag{17}$$

where V_e^b is the bending-related component of the rotation (due to M_e and H_e), while V_e^m is the membrane-solution component of the rotation. Making use of expression (12a), we may rewrite eq. (17) as

$$-\frac{1}{Et^2}[6(1-\nu^2)]^{1/2}[\omega_e M_e - \sqrt{2}(l\sin\alpha)H_e] + V_e^m = 0 \tag{18}$$

from which we obtain the result

$$M_e = \frac{1}{\omega_e}\left[\sqrt{2}(l\sin\alpha)H_e + \frac{Et^2 V_e^m}{\sqrt{6(1-\nu^2)}}\right] \tag{19}$$

If we make use of result (16) to eliminate H_e, and the membrane-solution result [6]

$$V_e^m = -\frac{3}{2}\frac{pl}{Et}\cot^2\alpha \tag{20}$$

to eliminate V_e^m, we may write the expression for M_e in the final form

$$M_e = \frac{p}{\omega_e}\left[\frac{l^2}{\sqrt{2}}\cos^2\alpha - \frac{3}{2}\frac{lt\cot^2\alpha}{\sqrt{6(1-\nu^2)}}\right] \tag{21}$$

4. Application to arbitrary cone-cone intersection

An arbitrary cone-to-cone intersection is depicted in Fig. 4, where subscripts 1 and 2 denote variables of the upper and lower cones respectively. Thus, the edge

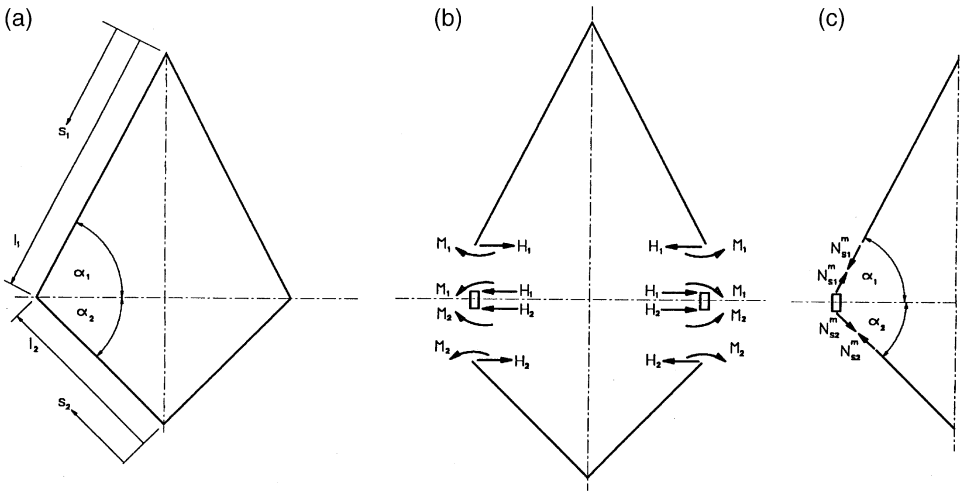

Fig. 4. Arbitrary cone-cone shell assembly: (a) general arrangement; (b) shell-edge bending and shearing actions; (c) shell-edge membrane actions.

redundants for the upper shell are now $\{M_1, H_1\}$, while those for the lower shell are $\{M_2, H_2\}$ (Fig. 4b). Similarly, the membrane meridional stress resultant occurring at the shell edge is now N_{s1}^{m} for the upper shell, and N_{s2}^{m} for the lower shell (Fig. 4c). The geometric parameters $\{l_1, \alpha_1, l_2, \alpha_2\}$ are arbitrary, so are the applied surface loadings on the two shells. In general, and unless proven otherwise, $M_1 \neq M_2$, $H_1 \neq H_2$ and $N_{s1}^{m} \neq N_{s2}^{m}$. We seek to derive generalised results for the shell-edge redundants $\{M_1, H_1, M_2, H_2\}$ in terms of the membrane stress resultants $\{N_{s1}^{m}, N_{s2}^{m}\}$ at the shell edges, the membrane edge deformations $\{V_1^{m}, \delta_1^{m}, V_2^{m}, \delta_2^{m}\}$, and the geometric parameters $\{l_1, \alpha_1, t_1, \omega_1, l_2, \alpha_2, t_2, \omega_2\}$ of the two shells, all these quantities being assumed to be known for a given cone-cone assembly under a given applied surface loading.

Horizontal-force and moment equilibrium of an element of the shell at the junction of the two cones (refer to Fig. 4b and c) yield

$$H_1 + H_2 - (N_{s1}^{m}\cos\alpha_1 + N_{s2}^{m}\cos\alpha_2) = 0 \tag{22a}$$

$$M_1 - M_2 = 0 \tag{22b}$$

from which we obtain the relationships

$$H_2 = (N_{s1}^{m}\cos\alpha_1 + N_{s2}^{m}\cos\alpha_2) - H_1 \tag{23a}$$

$$M_2 = M_1 \tag{23b}$$

Compatibility of deformations between the upper and lower shells (at their junction) requires that

$$V_1^{T} \,(= V_1^{b} + V_1^{m}) = -V_2^{T} \,(= -V_2^{b} - V_2^{m}) \tag{24a}$$

$$\delta_1^{T} \,(= \delta_1^{b} + \delta_1^{m}) = \delta_2^{T} \,(= \delta_2^{b} + \delta_2^{m}) \tag{24b}$$

The different origins for the distance coordinate s_1 (for shell 1) and s_2 (for shell 2) implies that positive rotations in the respective shells at their junction are actually opposed in sense (one is clockwise if the other is anticlockwise), hence the minus sign in the first of the above equations. On the other hand, positive lateral displacements in the respective shells at their junction are in the same direction (both point away from the common axis of revolution of the two shells), hence a minus sign is not required in the second equation.

Making use of results (12) to write these equations in expanded form, we obtain

$$-\frac{1}{Et_1^2}[6(1-\nu^2)]^{1/2}[\omega_1 M_1-\sqrt{2}(l_1\sin\alpha_1)H_1] + V_1^{\mathrm{m}} \tag{25a}$$

$$-\frac{1}{Et_2^2}[6(1-\nu^2)]^{1/2}[\omega_2 M_2-\sqrt{2}(l_2\sin\alpha_2)H_2] + V_2^{\mathrm{m}} = 0$$

$$\frac{\cos\alpha_1\cot\alpha_1}{4Et_1}\{\omega_1^2 M_1-2\sqrt{2}(l_1\sin\alpha_1)(\omega_1-\nu\sqrt{2})H_1\} + \delta_1^{\mathrm{m}} \tag{25b}$$

$$= \frac{\cos\alpha_2\cot\alpha_2}{4Et_2}\{\omega_2^2 M_2-2\sqrt{2}(l_2\sin\alpha_2)(\omega_2-\nu\sqrt{2})H_2\} + \delta_2^{\mathrm{m}}$$

Solving the above two simultaneous equations and simplifying, we finally obtain the following closed-form results:

$$M_1 = \tag{26a}$$

$$\frac{(\sin\alpha_1)(\sin\alpha_2)\{\xi F_1 + \sqrt{2}(t_1^2 l_2\sin\alpha_2-t_2^2 l_1\sin\alpha_1)(F_2-F_3)\}}{\eta F_1(\sin\alpha_1)(\sin\alpha_2) + \sqrt{2}(t_1^2 l_2\sin\alpha_2-t_2^2 l_1\sin\alpha_1)(t_2\omega_1^2\sin\alpha_2\cos^2\alpha_1-t_1\omega_2^2\sin\alpha_1\cos^2\alpha_2)}$$

$$H_1 = \tag{26b}$$

$$\frac{\xi(t_2\omega_1^2\sin\alpha_2\cos^2\alpha_1-t_1\omega_2^2\sin\alpha_1\cos^2\alpha_2)-\eta(\sin\alpha_1)(\sin\alpha_2)(F_2-F_3)}{\eta F_1(\sin\alpha_1)(\sin\alpha_2) + \sqrt{2}(t_1^2 l_2\sin\alpha_2-t_2^2 l_1\sin\alpha_1)(t_2\omega_1^2\sin\alpha_2\cos^2\alpha_1-t_1\omega_2^2\sin\alpha_1\cos^2\alpha_2)}$$

where

$$F_1 = t_1 l_2(\cos^2\alpha_2)(2\sqrt{2}\omega_2-4\nu) + t_2 l_1(\cos^2\alpha_1)(2\sqrt{2}\omega_1-4\nu) \tag{27a}$$

$$F_2 = 4Et_1 t_2(\delta_2^{\mathrm{m}}-\delta_1^{\mathrm{m}}) \tag{27b}$$

$$F_3 = t_1 l_2(\cos^2\alpha_2)(2\sqrt{2}\omega_2-4\nu)(N_{s1}^{\mathrm{m}}\cos\alpha_1 + N_{s2}^{\mathrm{m}}\cos\alpha_2) \tag{27c}$$

$$\xi = \sqrt{2}t_1^2(l_2\sin\alpha_2)(N_{s1}^{\mathrm{m}}\cos\alpha_1 + N_{s2}^{\mathrm{m}}\cos\alpha_2) + \frac{Et_1^2 t_2^2}{\sqrt{6(1-\nu^2)}}(V_1^{\mathrm{m}} + V_2^{\mathrm{m}}) \tag{27d}$$

$$\eta = \omega_1 t_2^2 + \omega_2 t_1^2 \tag{27e}$$

With M_1 and H_1 now known, the redundants of the lower cone, M_2 and H_2, immediately follow from relations (23).

The interior stress resultants $\{N_s^b, N_\theta^b\}$ and interior bending moments $\{M_s, M_\theta\}$ associated with the edge effects then follow from relations (11), when $\{M_e, H_e\}$ are replaced with the now known $\{M_1, H_1\}$ for the upper shell and $\{M_2, H_2\}$ for the lower shell.

The final stress distribution for the inner and outer surfaces of the shell are obtained by superimposing the stresses associated with the edge effects with the stresses associated with the membrane solution, as follows:

$$\sigma_s^T = \frac{N_s^b}{t} \pm \frac{6M_s}{t^2} + \frac{N_s^m}{t} \tag{28a}$$

$$\sigma_\theta^T = \frac{N_\theta^b}{t} \pm \frac{6M_\theta}{t^2} + \frac{N_\theta^m}{t} \tag{28b}$$

where σ_s^T refers to the meridional stresses, σ_θ^T refers to the hoop stresses, and t is, of course, the shell thickness. This then completes the stress analysis for the cone-cone problem.

5. Numerical example

Let us consider a large elevated concrete water tank in the form of a shell of revolution comprising two identical cones with $\alpha_1 = \alpha_2 = 60°$ and $l_1 = l_2 = 20$m (refer to Fig. 1 for these parameters). The tank is filled to capacity with water of weight $\gamma = 9810\text{N/m}^3$, and is axisymmetrically supported above the ground at some level close to the vertex of the lower cone. The thickness of the shell is constant at 0.2 m throughout (that is, $t_1 = t_2 = 0.2$m). Young's modulus of the concrete is taken as $E = 28 \times 10^9 \mathbf{N}/\text{m}^2$, while Poisson's ratio is taken as $\nu = 0.15$.

Fig. 5 shows the stress distribution in the meridional section of the tank, obtained on the basis of the closed-form analytical results presented in this paper. For both meridional-stress variations (Fig. 5a) and hoop-stress variations (Fig. 5b), the coordinate $s = 20$m corresponds to the (equatorial) junction of the two cones making up the rhombic tank. Plots to the left of the vertical line corresponding to the junction location refer to the upper cone, for which s is taken from zero (the apex) to 20 m (the junction location); those to the right of the vertical line refer to the lower cone, for which s is taken from 20 m (the junction location) down to 2 m. For the lower cone, it should be noted that stress variations are not shown for values of s smaller than 2 m, since the tank is supported somewhere in the neighbourhood of this location, making the real state of stress in this region quite dissimilar to that yielded by the analytical expressions in this paper. However, this should not be seen as a problem, as we are primarily concerned here with the state of stress around the cone-cone junction, which is sufficiently remote from the supports to render the effects of the latter (on the stress distribution around the cone-cone intersection) insignificant. For both meridional and hoop stress variations, inner and outer-surface total-stress plots ($\sigma^T(i)$ and $\sigma^T(o)$) are shown in relation to the membrane stress plots (σ^m).

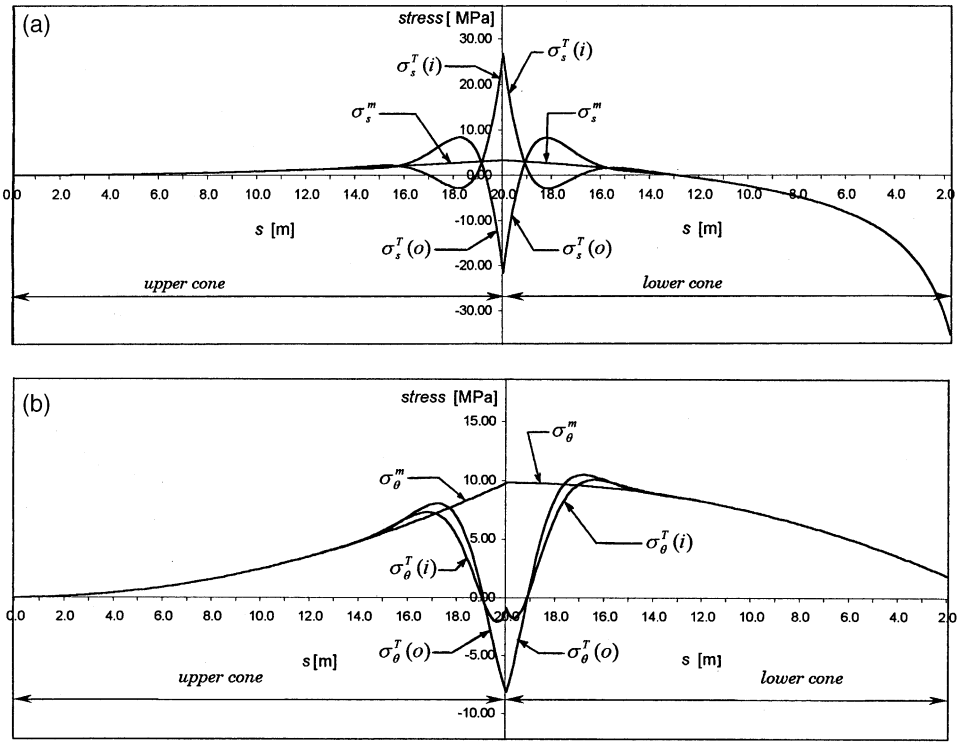

Fig. 5. Stress distribution in a water-filled rhombic shell of revolution with $l_1 = l_2 = 20$m and $\alpha_1 = \alpha_2 = 60°$: (a) meridional stresses; (b) hoop stresses.

As expected, the state of stress is essentially membrane away from the junction of the cones, but as the junction is approached from either the top or the bottom, the state of stress in the shell departs markedly from the membrane state of stress, reflecting the localised and rapidly changing character of bending effects. At the junction, and by reference to the meridional stresses first, the membrane solution predicts a stress of +3.27 N/mm^2 (tensile), yet the actual stresses as predicted by the combined membrane and bending solution are +26.64 N/mm^2 (tensile) for the inner surface and −21.73 N/mm^2 (compressive) for the outer surface. With regard to the hoop stresses, and again focussing attention on the junction location, the membrane solution predicts a stress of +9.81 N/mm^2 (tensile), whereas the actual stresses as given by the net solution (membrane + bending-disturbance) are −0.92 N/mm^2 (compressive) for the inner surface and −8.17 N/mm^2 (compressive) for the outer surface.

The relatively high magnitudes of the actual stresses versus membrane values vividly illustrate the importance of taking into account bending effects at the cone-cone shell junction, as these have a very strong (albeit localised) influence on the real state of stress in the shell. In this particular example, the combined analytical solution (membrane + bending effects) reveals tensile and compressive meridional

stresses at the junction that are several times greater than the membrane solution predicts, whereas for hoop stresses, the bending disturbance at the cone-cone junction has the effect of sharply reversing fairly substantial tensile membrane stresses at the junction into negative (compressive) net stresses. The latter tendency may be beneficial for a material like concrete which is much stronger in compression than it is in tension, as long as the possibility of local buckling is precluded. Clearly, in the case of the material concrete, the relatively large values of tensile meridional stresses (in excess of 20 N/mm^2) noted at the junction would require special measures aimed at either reducing them (e.g. by shell-thickness enhancement and/or prestressing of the concrete) or enhancing the capacity of the shell to sustain these (e.g. by using high-strength concrete and/or providing adequate steel reinforcement).

The reliability of the developed formulation has been demonstrated by analysing the same problem using the finite-element programme ABAQUS [9]. In the finite-element analysis, two-noded (conical) axisymmetric shell bending elements were used to model the conical profile, these being 100 in each of the top and bottom parts of the tank, with a uniform mesh density. The assembly therefore consisted of 200 elements and 201 nodes in total, each element being 200 mm in length. Hydrostatic pressure loading was prescribed upon the elements, with self-weight loading suppressed. To allow the analysis to proceed, the tank was provided with fully fixed support conditions at a distance of $s = 2$m from the vertex of the lower cone, but of course (and as already pointed out earlier) the precise nature of the support conditions is immaterial in our present assessment of the state of stress in the neighbourhood of the cone-cone junction, since the supports are sufficiently remote from the junction to significantly influence the stress pattern in the latter's vicinity.

Table 1 shows analytical results (upper row) versus FEM results (lower row) for inner and outer-surface meridional and hoop net stresses at the apex of the configuration ($s_1 = 0$), in the upper cone at a distance along the meridian of 2 m from the

Table 1
Analytical versus finite-element method (FEM) results for the numerical example. Analytical results appear in the upper row; FEM results are shown in the lower row in square brackets.

Location		σ_s (N/mm^2)		σ_θ (N/mm^2)	
s	Node no.	Inner	Outer	Inner	Outer
$s_1 = 0$	1	0.00	0.00	0.00	0.00
		[0.07]	[0.06]	[0.04]	[0.04]
$s_1 = 18$m	91	−2.75	+8.11	+5.15	+6.78
		[−2.86]	[+8.22]	[+5.24]	[+6.95]
$s_1 = 20$m	101	+26.64	−21.73	−0.92	−8.17
		[+27.29]	[−21.26]	[−0.55]	[−7.85]
$s_2 = 20$m	101	+26.64	−21.73	−0.92	−8.17
		[+26.99]	[−22.06]	[−0.50]	[−7.59]
$s_2 = 18$m	111	−2.85	+8.01	+6.91	+8.54
		[−2.63]	[+7.81]	[+6.41]	[+8.15]
$s_2 = 10$m	151	−2.45	−2.45	+7.36	+7.36
		[−2.54]	[−2.11]	[+6.98]	[+7.07]

junction ($s_1 = 18$m), in the upper cone right at the junction ($s_1 = 20$m), in the lower cone right at the junction ($s_2 = 20$m), in the lower cone at a distance along the meridian of 2 m from the junction ($s_2 = 18$m), and in the lower cone at a distance along the meridian of 10 m from the junction ($s_2 = 10$m). Here, and consistent with earlier notation, subscripts 1 and 2 associated with the distance coordinate s refer to the upper and lower cone respectively, the distance s itself being, of course, measured from the vertex of the cone in question. For the larger stress values at the junction (which are most critical), the discrepancy between the analytical results and the FEM results is generally less than 5%, showing that the closed-form analytical results derived and presented in this study are reliable for most practical engineering calculations.

6. Summary and concluding remarks

The problem of a conical shell axisymmetrically intersecting another conical shell, such that the vertices of the cones lie on opposite sides of the plane of intersection, has been considered. On the basis of the one-term asymptotic-series solution for the axisymmetric bending of a non-shallow conical shell, closed-form results have been derived for the discontinuity effects around the shell intersection, for arbitrary loading and geometric parameters of the intersecting cones.

The obtained generalised results are particularly useful in evaluating stresses and deformations in double-cone pressure vessels and liquid-retaining vessels with intersecting conical portions. They are applicable for both complete cones and the larger ends of conical frusta that are not 'too short', provided that $\alpha \geq 30°$ and $l/t \geq 30$, and provided that the shell thickness does not change appreciably in the narrow edge zone of the shell.

As an example of the application of the developed formulation, the stress distribution around the equatorial location of a relatively large liquid-filled rhombic shell of revolution has been evaluated, and some interesting observations made. The stresses obtained on the basis of the developed analytical approach have been shown to be in good agreement with those obtained from a finite-element analysis, thus validating the theoretical results given in the paper.

Acknowledgements

The assistance of Daniel Murambadoro with the preparation of the illustrations featured in this paper is gratefully acknowledged.

References

[1] Zingoni A. On the possibility of parabolic ogival shells for egg-shaped sludge digesters. In: Zingoni A, editor. Structural engineering, mechanics and computation, vol. 1. Oxford: Elsevier Science; 2001. p. 515–24.

[2] Zingoni A. Stresses and deformations in egg-shaped sludge digesters: membrane effects. Eng Struct 2001;23(11):1365–72.
[3] Zingoni A. Stresses and deformations in egg-shaped sludge digesters: discontinuity effects. Eng Struct 2001;23(11):1373–82.
[4] Timoshenko SP, Woinowsky-Krieger S. Theory of plates and shells. New York: McGraw-Hill, 1959.
[5] Flügge W. Stresses in shells. Berlin: Springer, 1973.
[6] Zingoni A. Shell structures in civil and mechanical engineering. London: Thomas Telford, 1997.
[7] Gould PL. Analysis of plates and shells. Englewood Cliffs, NJ: Prentice-Hall, 1998.
[8] Baltrukonis JH. Influence coefficients for edge-loaded short thin conical frustums. ASME J Appl Mech 1959;26:2.
[9] ABAQUS standard user's manual (version 5.8). New York: Hibbitt, Karlsson and Sorensen Inc.; 1998.